



Safar, F., Hurdiss, E., Erotocritou, M., Greiner, T., Lape, R., Irvine, M. W., Fang, G. Y., Jane, D., Yu, R., Dämgen, M. A., Biggin, P. C., & Sivilotti, L. G. (2017). The Startle Disease Mutation E103K Impairs Activation of Human Homomeric $\alpha 1$ Glycine Receptors by Disrupting an Intersubunit Salt Bridge across the Agonist Binding Site. *Journal of Biological Chemistry*, 292(12), 5031-5042.
<https://doi.org/10.1074/jbc.M116.767616>

Publisher's PDF, also known as Version of record

License (if available):
CC BY

Link to published version (if available):
[10.1074/jbc.M116.767616](https://doi.org/10.1074/jbc.M116.767616)

[Link to publication record in Explore Bristol Research](#)
PDF-document

This is the final published version of the article (version of record). It first appeared online via *Journal of Biological Chemistry* at <https://doi.org/10.1074/jbc.M116.767616>. Please refer to any applicable terms of use of the publisher.

University of Bristol - Explore Bristol Research

General rights

This document is made available in accordance with publisher policies. Please cite only the published version using the reference above. Full terms of use are available:
<http://www.bristol.ac.uk/red/research-policy/pure/user-guides/ebr-terms/>

The Startle Disease Mutation E103K Impairs Activation of Human Homomeric $\alpha 1$ Glycine Receptors by Disrupting an Intersubunit Salt Bridge across the Agonist Binding Site*

Received for publication, November 14, 2016, and in revised form, January 25, 2017. Published, JBC Papers in Press, February 7, 2017, DOI 10.1074/jbc.M116.767616

Fatemah Safar^{†1}, Elliot Hurdiss^{†2}, Marios Erotocritou[†], Timo Greiner[†],  Remigijus Lape[†], Mark W. Irvine[§], Guangyu Fang[§], David Jane[§], Riley Yu^{||}, Marc A. Dämgen^{||3},  Philip C. Biggin^{||}, and  Lucia G. Sivilotti^{†4}

From the [†]Department of Neuroscience, Physiology and Pharmacology, University College London, Gower Street, London WC1E 6BT, United Kingdom, the ^{||}Department of Biochemistry, Structural Bioinformatics and Computational Biochemistry, University of Oxford, South Parks Road, Oxford OX1 3QU, United Kingdom, the [§]School of Physiology and Pharmacology, University of Bristol, University Walk, Bristol BS8 1TD, United Kingdom, and the ^{||}Key Laboratory of Marine Drugs, Chinese Ministry of Education, School of Medicine and Pharmacy, Ocean University of China, Qingdao 266003, China

Edited by Roger J. Colbran

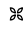
Glycine receptors (GlyR) belong to the pentameric ligand-gated ion channel (pLGIC) superfamily and mediate fast inhibitory transmission in the vertebrate CNS. Disruption of glycinergic transmission by inherited mutations produces startle disease in man. Many startle mutations are in GlyRs and provide useful clues to the function of the channel domains. E103K is one of few startle mutations found in the extracellular agonist binding site of the channel, in loop A of the principal side of the subunit interface. Homology modeling shows that the side chain of Glu-103 is close to that of Arg-131, in loop E of the complementary side of the binding site, and may form a salt bridge at the back of the binding site, constraining its size. We investigated this hypothesis in recombinant human $\alpha 1$ GlyR by site-directed mutagenesis and functional measurements of agonist efficacy and potency by whole cell patch clamp and single channel recording. Despite its position near the binding site, E103K causes hyperekplexia by impairing the efficacy of glycine, its ability to gate the channel once bound, which is very high in wild type GlyR. Mutating Glu-103 and Arg-131 caused various degrees of loss-of-function in the action of glycine, whereas mutations in Arg-131 enhanced the efficacy of the slightly bigger partial agonist sarcosine (*N*-methylglycine). The effects of the single charge-swapping mutations of these two residues were largely rescued in the double mutant, supporting the possibility that they interact via a salt bridge that normally constrains the efficacy of larger agonist molecules.

Ion channels that belong to the pentameric ligand-gated superfamily (pLGIC)⁵ are found both in prokaryotic and eukaryotic organisms. In vertebrates, including man, pLGIC mediate fast synaptic transmission both in the periphery (see for instance, the cation permeable, nicotinic ACh receptors at the neuromuscular junction) and in the central nervous system (*cf.* the inhibitory, anion-permeable GABA and glycine receptors). pLGIC are activated by the binding of agonist/neurotransmitters to canonical binding sites at the extracellular interface of two subunits. Each receptor type recognizes as agonists a fairly narrow range of ligand molecules. However, in the superfamily as a whole, the group of chemical structures that can activate these channels is remarkably diverse, from small amines such as ACh or propylamine, to amino acids (glycine, GABA, and glutamate), to aromatic compounds (histamine, serotonin, tyramine, and nicotine). How pLGIC achieve this level of agonist recognition is still an area of intense investigation (1).

Structural data from several pLGIC members show that channel subunits have a conserved fold and that the main structural features of the agonist binding site, as first hypothesized in the early 1990s (2), are shared across the superfamily. Thus, the site is made by “loops” A, B, and C from the outer β sheet of the anticlockwise (principal) subunit and by loops D to G from the inner β sheet of the clockwise (complementary) subunit. The loops contain many aromatic residues, an “aromatic box” (3, 4) whose side chains form cation- π interactions with the positively charged moiety of pLGIC agonists. The actual aromatic residues that make the “box” differ across pLGIC subtypes, and probably so does the size of the aromatic box (5).

Combining structural and functional data with homology modeling suggests that few of the loop residues form direct bonds with the agonist, whereas others contribute to holding these key residues in place (1, 6, 7). Which agonists are recognized and what sets their efficacy is likely to be influenced by

* This work was supported in part by Medical Research Council Project Grant MR/J007110/1 (to L. G. S. and P. C. B.). The authors declare that they have no conflicts of interest with the contents of this article.

 Author's Choice—Final version free via Creative Commons CC-BY license.

¹ Supported by a Kuwaiti state scholarship.

² Supported by a UCL Impact studentship (to L. G. S.).

³ Supported by an Oxford Wolfson Marriot Biochemistry Graduate Scholarship and the Studienstiftung des deutschen Volkes.

⁴ To whom correspondence should be addressed. Tel.: 44-20-76793880; Fax: 44-20-76797298; E-mail: l.sivilotti@ucl.ac.uk.

⁵ The abbreviations used are: pLGIC, pentameric ligand-gated ion channel superfamily; GlyR, glycine receptor; P_{open} , open probability; TEA, tetraethylammonium; PDB, Protein Data Bank.

other properties of the binding site, such as its size and flexibility both at rest and after activation, but we do not know how these are determined in the protein.

For pLGICs as for other channels, important clues about the function of the different structural domains have come from the discovery and characterization of channelopathy mutations that cause inherited disease in man. The human disease associated with impaired glycinergic transmission is called startle disease or hyperekplexia, and is caused most often by loss-of-function mutations of glycine receptors (GlyR), particularly in the $\alpha 1$ subunit (8). Startle disease mutations are thought to exert their effects largely by damaging receptor gating, namely how well the GlyR opens once it has bound the neurotransmitter glycine (9, 10). This hypothesis is largely based on the analysis of the first mutations to be characterized, such as K276E and Q266H (9–12). These residues are in the transmembrane domain of the channel, where the channel gate is and where most startle mutations are found. Relatively few startle mutations are in the receptor binding site and little is known of how they may act. If these disrupt binding, anything short of a profound disruption of agonist binding is unlikely to damage glycinergic synaptic transmission enough to produce a startle phenotype, because glycine in the synaptic cleft reaches high concentrations of 2.2–3.5 mM (13) and this should provide a safety margin. A recent report (14) has shown that a startle mutation lethal in the mouse, N46K $\alpha 1$ GlyR (near the principal side of the binding site) may exert its effects by speeding up GlyR deactivation. Startle mutations that are in the binding site and do not abolish agonist binding may be particularly interesting to investigate, as they are likely to act by interfering with the transduction of the agonist binding signal toward the pore. This “gating aspect” of the binding site function is poorly understood, but important, as it must contribute to how agonist efficacy is determined.

The startle mutation E103K in loop A, on the principal side of the binding pocket (Fig. 1, A and B), was first described in a patient whose second $\alpha 1$ allele carried a frameshift mutation (15). Our homology model of the GlyR (7) based on the structure of GluCl (16) suggested that the side chain of Glu-103 is likely to form a salt bridge across the binding site with Arg-131 in loop E of the complementary subunit. To our knowledge, no hyperekplexia mutations have been reported for Arg-131. Molecular dynamics simulations on a new model built on the recent cryo-EM structure of the zebrafish $\alpha 1$ GlyR (17) confirm that the salt bridge is present and show that it is conformationally stable (at least on a 500-ns time scale). In the present study we confirmed the interaction between these two residues and found that, despite its binding site location, the hyperekplexia E103K mutation affected only glycine efficacy. The effect of mutating Glu-103 and Arg-131 was different for the full agonist glycine and the bulkier, partial agonist sarcosine.

Results

The Hyperekplexia Mutation E103K Decreases Both the Potency and the Efficacy of Glycine on $\alpha 1$ GlyR—Fig. 1A shows the position of the Glu-103 residue in a view taken from the GlyR homology model (7) that we produced (cyan) from the structure of GluCl (34% sequence identity with the $\alpha 1$ GlyR

(16). Glu-103 is located at (or near) loop A of the principal (+) subunit (on the *left* in Fig. 1A, *orange* in Fig. 1C), and its negatively charged side chain is near the positively charged side chain of Arg-131 in loop E on the complementary (–) side of the binding site (on the *right* in Fig. 1A, *purple* in Fig. 1C). In the model, distances between side chain hydrogen atoms of Arg-131 to the side chain oxygen atoms of Glu-103 are 2.5–2.8 Å, a range compatible with the presence of a salt bridge, which conceivably might have a stabilizing effect both on loops A and E and tighten the size of the binding site. The homology model is very similar to the structure of the zebrafish $\alpha 1$ GlyR (*green* in Fig. 1A; Protein Data Bank (PDB) code 3JAE) (17), where the position of the side chains of the two amino acids is not well defined. To investigate this further we performed molecular dynamics simulations (500 ns each for glycine and sarcosine bound) on a new model of human $\alpha 1$ GlyR based upon the zebrafish $\alpha 1$ GlyR structure (with glycine bound; PDB code 3JAE) (17); the domains in the structure have 94% sequence identity with the human $\alpha 1$ GlyR). In both cases the salt bridge was conformationally stable and present for at least 90% of the simulation time (90% for glycine bound and 97% for sarcosine) as averaged for all five binding pockets. The binding modes and salt bridge behavior were similar for glycine and sarcosine (Fig. 1C, *left* and *right*).

Glu-103 and Arg-131 are at the back of the binding site, toward the extracellular vestibule of the pore. Glu-103 is adjacent to residue Lys-104, whose charged side chain is likely to be exposed to the pore vestibule, and is one of the conductance determinants in pLGIC channels (18, 19). In our model, the charged side chains of both Glu-103 and Arg-131 are far from the center of the pore, at a distance of ~16 Å, and are not exposed to the interior of the pore. Thus, it is unlikely that Glu-103 and Arg-131 affect conductance directly, but we cannot exclude that mutating either residue may change conductance by perturbing the position of nearby residue Lys-104.

Interestingly, both the GluCl and the zebrafish homology models show that Glu-103 and Arg-131 residues are also at some distance from the agonist (~8 Å from glycine for example; data not shown), and thus any direct interaction with the agonist is expected to be minor as well. Any effects are therefore likely to be indirect, and to be exerted by affecting other residues, which do form direct bonds with glycine, such as loop A Phe-99 or loop E Ser-129. The salt bridge between Glu-103 and Arg-131 might be needed to maintain the correct conformation of loop A, which in turn influences the direct bonds of other residues with the agonist. An alignment of the amino acid sequences in loops A and E of nine pLGIC channels is shown in Fig. 1B. The Glu/Arg pair of residues in these locations are conserved in a subset of the inhibitory pLGIC receptors, namely all the GlyR subunits ($\alpha 1$ –4 and β), irrespective of species, in *Caenorhabditis elegans* GluCl and in a few GABA receptor subunits, but is absent in the cationic channels (nicotinic, 5-HT₃, GLIC, and ELIC).

In light of our considerations from the homology models, and our hypothesis that a salt bridge between Glu-103 and Arg-131 stabilizes loops A and E and tightens the binding site, we decided to test the effects of the E103K startle mutation on the

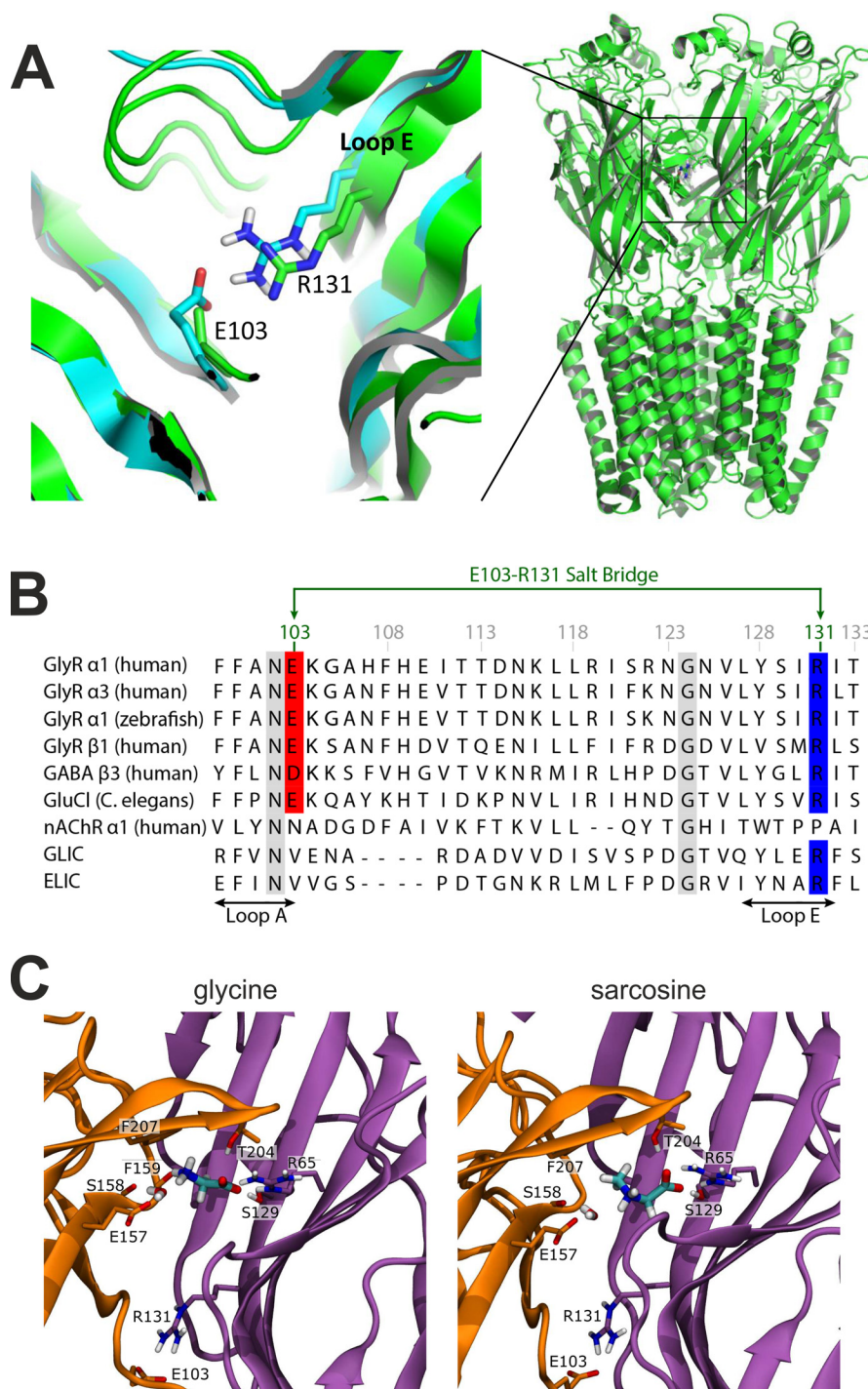


FIGURE 1. Homology modeling reveals a salt-bridge between residues Glu-103 and Arg-131. *A*, location of the Glu¹⁰³-Arg¹³¹ salt-bridge as predicted by a GlyR homology model (cyan) (7) built using GluCl as template (PDB code 2XY5) (16). The model is overlaid with the recent cryo-EM structure (green) of the zebrafish α 1 GlyR (PDB 3JAE) (17). Note that the Glu-103 side chain is not fully resolved in the cryo-EM structure, but is certainly within distance to form the salt bridge as postulated by the model. *B*, an amino acid alignment of this region for nine members of the pLGIC superfamily showing the position of the salt bridge between Glu-103 (red) and Arg-131 (blue) and its conservation in glycine receptors. Other conserved positions are indicated by a gray background. *C*, the agonist binding mode and the Glu¹⁰³-Arg¹³¹ salt bridge in a GlyR homology model based on the zebrafish α 1 GlyR structure (PDB 3JAE) (17). Glycine (left) and sarcosine (right) are shown in the final frame after 500 ns simulation time. Orange, principal subunit; purple, complementary subunit. For both ligands, the carboxyl group is sandwiched by hydrogen bonds with Thr-204 and Ser-129 and is further stabilized by a salt bridge with Arg-65. The ammonium moiety interacts with a water molecule in the binding pocket, and the water is stabilized by hydrogen bonds to Glu-157 and to the backbone carbonyl oxygen of Ser-158 (as in Ref. 7). The ammonium group of glycine engages in an additional cation- π interaction with Phe-207 and forms a hydrogen bond with the backbone carbonyl group of Phe-159. This is sterically hindered for sarcosine by its additional *N*-methyl group.

GlyR responds to the full agonist glycine and to the partial agonist sarcosine (20). Sarcosine (*N*-methylglycine) is slightly bulkier than glycine (see the structures of the two agonists in

Fig. 1C) because of the methyl group substitution on the amino group, which is likely to be oriented toward the back of the binding site (7).

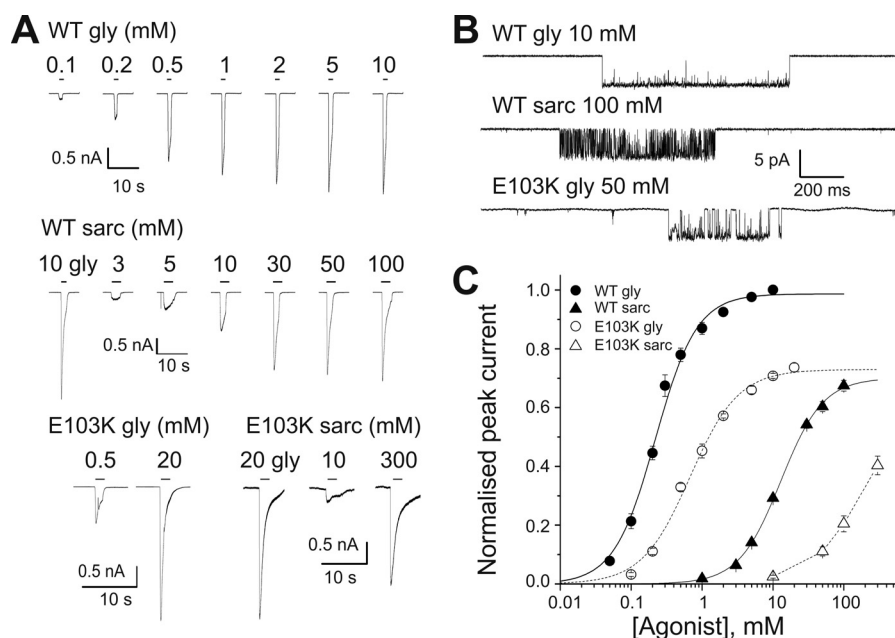


FIGURE 2. The E103K startle mutation reduces the sensitivity of $\alpha 1$ GlyR to both glycine and sarcosine and impairs channel gating. *A*, representative whole-cell current responses evoked by U-tube agonist application to HEK 293 cells expressing WT $\alpha 1$ GlyR (upper panels, 2 different cells) or E103K $\alpha 1$ GlyR (lower panel, 2 different cells). Black bars above the traces show the timing of the applications. Panels also show the responses to a saturating concentration of glycine obtained in the cells used for the sarcosine concentration-response curves. *B*, clusters of single channel activity elicited by saturating concentrations of glycine (upper panel) or sarcosine (middle panel) on WT $\alpha 1$ GlyR or (glycine only) on E103K GlyR (lower panel; cell-attached configuration, channel openings downwards). Note the decreased single channel P_{open} in mutant receptors. *C*, whole cell concentration-response curves to glycine and sarcosine in WT ($n = 7$ and 10, respectively) and E103K $\alpha 1$ GlyR ($n = 4$ and 3, respectively). Curves are scaled to the maximum single channel P_{open} measured at saturating glycine or sarcosine; for sarcosine on E103K GlyR, we could not measure the maximum single channel P_{open} and the curve is scaled indirectly (e.g. responses to sarcosine are scaled to the macroscopic maximum response to glycine in the same cell, and then scaled to the maximum glycine single channel P_{open}).

We began our investigation by obtaining whole cell concentration-response curves from HEK 293 cells expressing homomeric GlyR. Fig. 2*A* shows typical currents responses for the wild type $\alpha 1$ GlyR (top two panels) and the E103K mutant (bottom panel) to the agonists glycine and sarcosine. Glycine is a full agonist on homomeric $\alpha 1$ GlyR (21), but the traces in Fig. 2*A* (middle panel) show that sarcosine is a partial agonist, and its maximum current responses reach only 80% of those to glycine when the agonists are applied to the same cell at saturating concentrations (10 mM for glycine and 100 mM for sarcosine; Table 1). The time course of the currents was similar for both agonists, and desensitization became apparent at EC_{30} – EC_{50} for both glycine and sarcosine on WT and mutant receptors.

The E103K mutation reduced the channel sensitivity to agonists. The effect was relatively small for glycine, whose EC_{50} increased from 0.23 ± 0.02 to 0.71 ± 0.11 mM ($n = 10$ and 3, respectively; Fig. 2*A*, filled and hollow circles in Fig. 2*C*; Table 1). The loss of potency of sarcosine was much greater. In the mutant this prevented us from obtaining a full sarcosine dose-response curve (because of the very high concentrations required to saturate the curve). Thus we could not establish whether the mutation changed the sarcosine maximum response relative to glycine. Such a decrease in the relative maximum response to a partial agonist would have been the simplest way to check whether this binding site mutation impairs channel gating.

An even better way to assess whether a mutation has an effect on gating is to measure the channel maximum open probability in single channel records. The measurement of cluster open probability has the advantage (versus whole cell macroscopic

responses curves) of measuring an absolute open probability value that is not affected by the level of expression of the different channels examined or by changes in the channel conductance produced by the mutations. In addition, cluster open probability measures only changes in receptor activation and is not affected by desensitization (as desensitized intervals are not included in the analysis). Because of that, in Fig. 2*C* (and the following figures) we display concentration-response curves as whole cell responses scaled to the maximum open probability measured by single channel analysis.

The traces in Fig. 2*B* show clusters of single channel activity in cell-attached patches at saturating agonist concentrations. The glycine traces (top) show that the channel exposed to 10 mM glycine is practically either desensitized or open all the time, with a very high maximum P_{open} of 0.987 ± 0.002 ($n = 49$ clusters from 9 patches; measured as cluster open time/total cluster time), confirming that glycine is a very efficacious agonist on WT homomeric GlyR (21). In agreement with the whole cell data, single-channel WT clusters activated by a saturating sarcosine concentration (100 mM; Fig. 2*B*, middle trace) have a lower maximum P_{open} of 0.70 ± 0.03 ($n = 22$) and therefore confirm that sarcosine is a partial agonist in WT GlyR. The bottom trace of Fig. 2*B* shows channel activity evoked by glycine in the E103K mutant. These openings show that the mutation did not affect conductance, as their amplitude is similar to that of WT channels (right-hand column in Table 1). Mutating the adjacent residue Lys-104 to glutamate produces a 22% conductance decrease in the $\alpha 1$ homomeric GlyR, but Lys-104 is likely to be exposed to the channel pore (18). Mutant channel activity showed distinct clustering, with an open probability of $0.73 \pm$

TABLE 1

Properties of wild type and mutant human recombinant $\alpha 1$ GlyR in patch clamp experiments

	Whole cell dose-response curves					Single channel measurements			
	EC ₅₀	I _{max}	I _{max} /I _{GLY max}	n _H	n	Concentration	maxP _{open} (# clusters)	Amplitude	n
	mM	nA				mM		pA	
Glycine									
WT	0.23 ± 0.02	8 ± 2	1.58 ± 0.07	10	10	10	0.987 ± 0.002 (49)	5.2 ± 0.2	9
E103K	0.71 ± 0.11	2.7 ± 1.4	1.32 ± 0.06	3	3	50	0.73 ± 0.07 (13)	5.2 ± 0.1	3
E103A	0.43 ± 0.05	5.9 ± 0.3	1.24 ± 0.06	3	3	100	0.97 ± 0.01 (11)	5.6 ± 0.2	3
E103R	1.4 ± 0.4	12.8 ± 1.6	0.78 ± 0.03	8	8	200	0.87 ± 0.02 (11)	5.8 ± 0.1	3
R131A	0.19 ± 0.03	8.7 ± 1.9	0.90 ± 0.01	5	5	30	0.95 ± 0.01 (16)	4.58 ± 0.04	2
R131E	1.6 ± 0.2	1.5 ± 0.3	1.6 ± 0.1	4	4	50	0.93 ± 0.02 (28)	3.90 ± 0.03	2
R131E/E103R	0.43 ± 0.04	3.7 ± 0.4	0.95 ± 0.02	5	5	100	0.996 ± 0.001 (9)	4.8 ± 0.1	5
Sarcosine									
WT	14 ± 1	5.1 ± 0.6	0.80 ± 0.03	1.51 ± 0.04	7	100	0.70 ± 0.03 (22)	5.6 ± 0.3	4
E103K	>80	1.5 ± 0.4	0.62 ± 0.04	1.37 ± 0.03	4	300	Very heterogeneous	4.2 ± 0.1	8
E103A	23 ± 3	5.1 ± 1.7	0.76 ± 0.03	1.8 ± 0.2	4	100	0.67 ± 0.08 (8)	4.5 ± 0.4	4
E103R	17 ± 3	2.6 ± 0.8	0.84 ± 0.09	1.22 ± 0.05	5	200	0.79 ± 0.03 (31)	5.0 ± 0.1	4
R131A	4.5 ± 0.5	6.0 ± 1.1	0.93 ± 0.02	1.4 ± 0.1	5	100	0.95 ± 0.01 (37)	5.4 ± 0.1	3
R131E	75 ± 2	6.6 ± 0.9	0.81 ± 0.03	2.05 ± 0.03	6	300	0.91 ± 0.04 (21)	4.7 ± 0.1	2
R131E/E103R	15 ± 2	8.1 ± 2.3	0.95 ± 0.04	1.28 ± 0.07	8	100	0.97 ± 0.01 (23)	4.9 ± 0.3	8

0.07 ($n = 13$) to saturating glycine. Single-channel activity of E103K mutants in response to 300 mM sarcosine was not informative, not only because we do not know whether this concentration produces maximum activation, but also because clusters were sometimes hard to define unambiguously and because there was substantial heterogeneity in the channel open probability from cluster to cluster (data not shown).

Thus single channel data confirm that the E103K mutation must impair channel gating elicited by the full agonist glycine. Many mutations that produce loss of gating function have similar effects on all agonists, but given the position of this mutation is near the binding site, we investigated this further.

The Effect of Mutating Residues Glu-103 and Arg-131 on the Agonist Action of Glycine and Sarcosine Is Different—To test the hypothesis that there is a salt bridge between Glu-103 and Arg-131, we mutated both residues individually to an alanine and also reversed the side chain charges, to arginine and glutamate, respectively.

Fig. 3 shows the effects of mutating either residue on responses to the full agonist glycine. Traces in *panel A* show that the time course of agonist responses was not affected by the mutations. There was a clear pattern of effects on the activity of glycine: shortening the residue side chain and removing its charge by replacing glutamate or arginine with alanine had only negligible effects in either the 103 or 131 positions. This was true for both the potency of glycine (Fig. 3C, Table 1) and for its efficacy, as both the E103A and R131A mutants maintained a high maximum P_{open} (0.97 ± 0.01 and 0.95 ± 0.01 , $n = 11$ and 16, respectively; *top traces* in Fig. 3B; Table 1).

The picture was different when the side chain charge was reversed. In R131E there was a substantial decrease in the channel sensitivity to glycine (to an EC₅₀ of 1.6 ± 0.2 mM, $n = 4$; Table 1) accompanied by a small decrease in maximum P_{open} (to 0.93 ± 0.02). A more marked effect was seen with E103R, where the increase in EC₅₀ (to 1.4 ± 0.4 mM, $n = 8$; Table 1) was associated with a clear reduction in the slope of the dose-response curve (from 1.58 ± 0.07 to 0.78 ± 0.03), an effect not seen with E103K. At 200 mM glycine, a concentration that should be maximal on the dose-response curve, the single chan-

nel P_{open} of E103R was 0.87 ± 0.02 (*cf.* 0.987 and 0.73 for WT and E103K, respectively; Table 1).

Fig. 4 shows that with the bulkier partial agonist sarcosine, the effect of the mutations depended mostly on their location. Mutating Glu-103 had only a small impact for both E103A and E103R. Thus we observed no shift, or a modest one, in macroscopic EC₅₀ and no clear change in maximum P_{open} (*left panels* in Fig. 4B; 0.70 ± 0.03 , 0.67 ± 0.08 , and 0.79 ± 0.03 for WT, E103A, and E103R, respectively; $n = 22$, 8, and 31 clusters). In contrast with that, both mutations of Arg-131 markedly increased the P_{open} of sarcosine-evoked clusters (*right-hand panels* in Fig. 4B) and turned sarcosine into a nearly full agonist. For the R131A mutation, the increase in maximum P_{open} (0.95 ± 0.04 , $n = 37$) was associated with an increase in sarcosine potency, and the EC₅₀ shifted from 14 mM (WT) to 4.5 ± 0.5 mM (Table 1; $n = 7$ and 5).

For R131E, we cannot be sure that the concentration-response curve is reaching its maximum at the highest concentration of sarcosine that we could test (300 mM). Nevertheless, this concentration elicited a P_{open} of $0.91 (\pm 0.04)$; $n = 21$; *cf. bottom left trace* of Fig. 4B), higher than the WT maximum value. Equally, the EC₅₀ in the mutant must be greater than 75 mM, and therefore sarcosine potency was decreased by at least 5-fold. Note that enhanced gating (proven by the increase in P_{open} in these mutants) *per se* should increase the potency of an agonist. As enhanced gating was accompanied instead by a sizeable decrease in potency, the R131E mutation must also decrease sarcosine affinity for the resting receptor.

Reversing the Side Chain Charges on Both Glu-103 and Arg-131: the Effect of the Double E103R/R131E Mutation on the Agonist Action of Glycine and Sarcosine—Fig. 5C (*left panel*) shows that the double E103R/R131E mutation substantially rescued the effects on receptor function of the single charge reversal mutants. This was particularly clear in the case of glycine, with an EC₅₀ in the double charge reversal mutant of 0.43 ± 0.04 mM (*black circles*, $n = 5$), close to the WT value of 0.23 mM (Fig. 5, A and C; *cf.* an EC₅₀ of 1.4 ± 0.4 mM for E103R and 1.6 ± 0.2 mM for R131E; shown as *dashed* and *dotted* curves in Fig. 5C; Table 1). The cluster single channel trace in Fig. 5B,

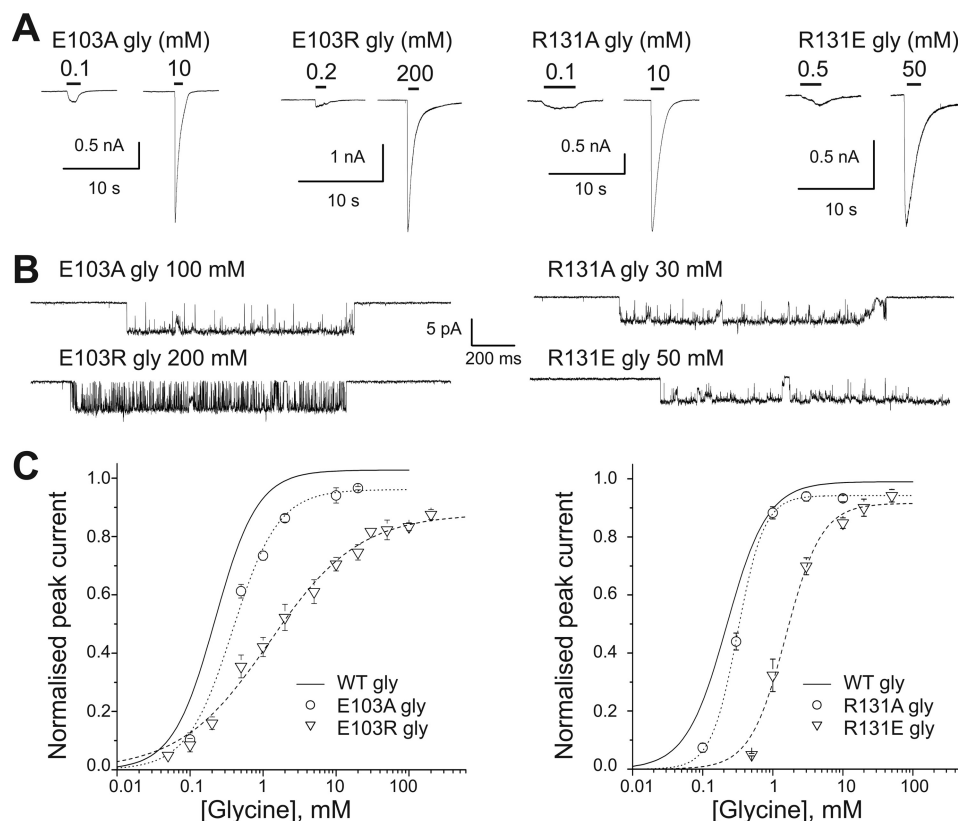


FIGURE 3. Reversing the side chain charge in positions Glu-103 or Arg-131 changes the potency and efficacy of glycine. *A*, representative whole cell current responses to glycine applied to GlyR $\alpha 1$ mutants. *B*, clusters of single-channel mutant GlyR activity elicited in cell-attached patches by saturating concentrations of glycine. *C*, whole cell concentration-response curves for the effect of glycine on E103A, E103R, R131A, and R131E mutant GlyR ($n = 3, 8, 5$, and 4, respectively). Curves are scaled to the maximum P_{open} obtained from single channel recordings. The WT concentration-response curve for glycine is shown for comparison (solid line; the data for this curve is shown in Fig. 2C).

top, shows that the maximum P_{open} elicited by glycine in the double mutant is also similar to that of WT GlyR (0.996 ± 0.001 and 0.987 ± 0.002 , $n = 9$ and 49, respectively).

The picture is slightly different for sarcosine. Here the double mutant has a sarcosine EC_{50} (Fig. 5, *A* and *C*) very similar to that of WT receptors (15 ± 2 and 14 ± 1 mM for the double mutant and wild type, respectively; *cf.* 17 ± 3 mM for E103R and at least 75 ± 2 mM for R131E). However, the maximum P_{open} elicited by sarcosine in the double mutant has remained high (0.97 ± 0.01) and resembles more the reverse charge mutant R131E (where the maximum P_{open} is at least 0.91 ± 0.04) than it does the WT receptor (0.70 ± 0.03). Thus, most of the effects of single charge reversal mutations of these residues are rescued by swapping their side chains, supporting the hypothesis that they form an intersubunit salt bridge.

Discussion

Our main finding is that residues Glu-103 in loop A and Arg-131 in loop E of the canonical GlyR agonist binding site are important determinants of agonist gating efficacy, and that their influence is agonist-dependent.

The Startle Disease Mutation E103K in Loop A of the Agonist Binding Site Acts by Impairing Glycine Gating—This mutation reduced the efficacy of the full agonist glycine on human $\alpha 1$ GlyR, as it decreased the maximum P_{open} produced by the amino acid from 0.987 to 0.73. This effect was associated with a relatively small loss in glycine potency, which brought the gly-

cine EC_{50} from 0.23 to 0.71 mM. This loss in potency can be entirely accounted for by the reduction in glycine efficacy. The reason is as follows. The maximum P_{open} measured in a single channel cluster depends only on effective efficacy E_{eff} (defined as in Ref. 22, as $EF/(EF + F + 1)$, where E is the opening equilibrium constant and F is the equilibrium constant for the pre-opening flip conformational change). Maximum $P_{\text{open}} = E_{\text{eff}}/(E_{\text{eff}} + 1)$. Our P_{open} data imply a decrease in E_{eff} of ~ 20 – 25 -fold (from 70 in WT receptors to 3 in the E103K GlyR). We know that the GlyR requires three molecules of agonist to open effectively (21) and we can therefore estimate that the 20-fold reduction in efficacy observed for E103K should by itself increase agonist EC_{50} by ~ 3 -fold (the cube root of 20) (23). This shift in EC_{50} is close to the one we observed in our experiments, and suggests that the E103K mutation does not cause major changes in the affinity of glycine for the binding site in its resting state.

This is in line with the structural information that Glu-103 does not contact the glycine molecule directly, and makes this residue particularly interesting, as it is a strong gating determinant for glycine, despite its position in the binding site. Differences in efficacy are translated into differences in gating, and reflect how much different agonists stabilize the active form of the channel. In pLGIC this is determined by the initial conformational changes and pre-open intermediate states (flip/primed/catch-and-hold) (22, 24–26). At the binding site, effi-

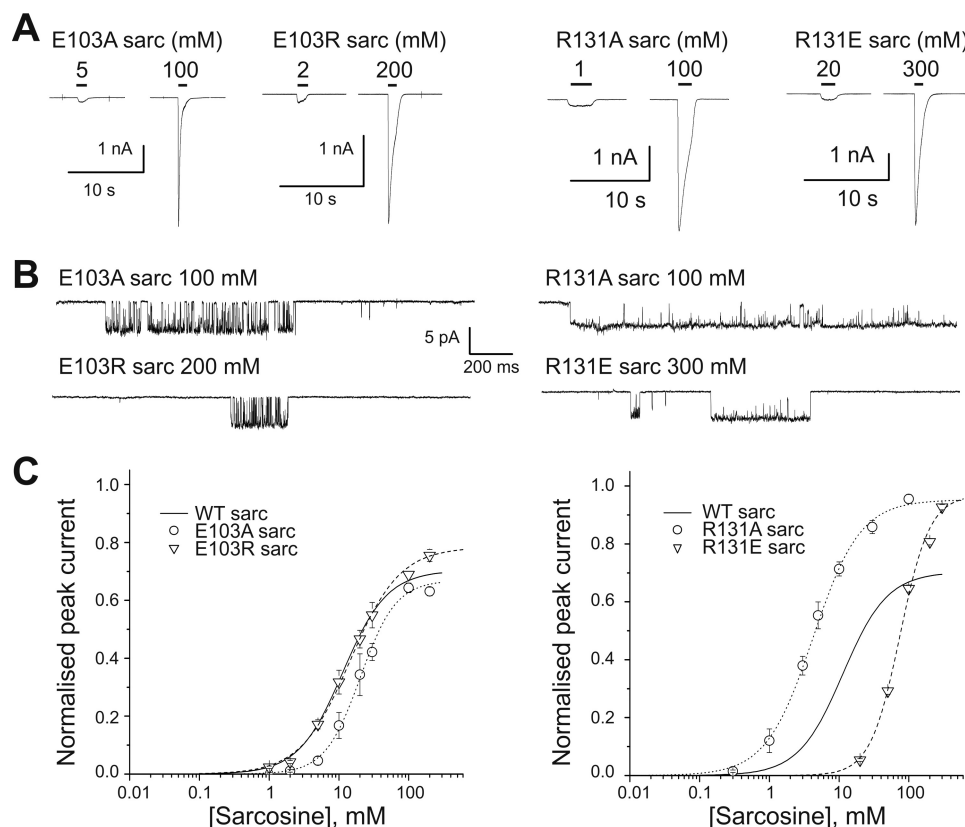


FIGURE 4. Removing or reversing the side chain charge of Arg-131 increases the efficacy of the partial agonist sarcosine on $\alpha 1$ GlyR. *A*, representative whole cell current responses to sarcosine in $\alpha 1$ GlyR mutants. *B*, clusters of single-channel mutant GlyR activity elicited in cell-attached patches by high concentrations of sarcosine (saturating except for the R131E mutant). *C*, sarcosine whole cell concentration-response curves for E103A, E103R, R131A, and R131E mutant GlyR ($n = 4, 4, 5$, and 6 , respectively). Curves are scaled to the appropriate maximum P_{open} measured by single channel recording. The WT concentration-response curve for sarcosine is shown for comparison (solid line; the data for this curve is shown in Fig. 2C).

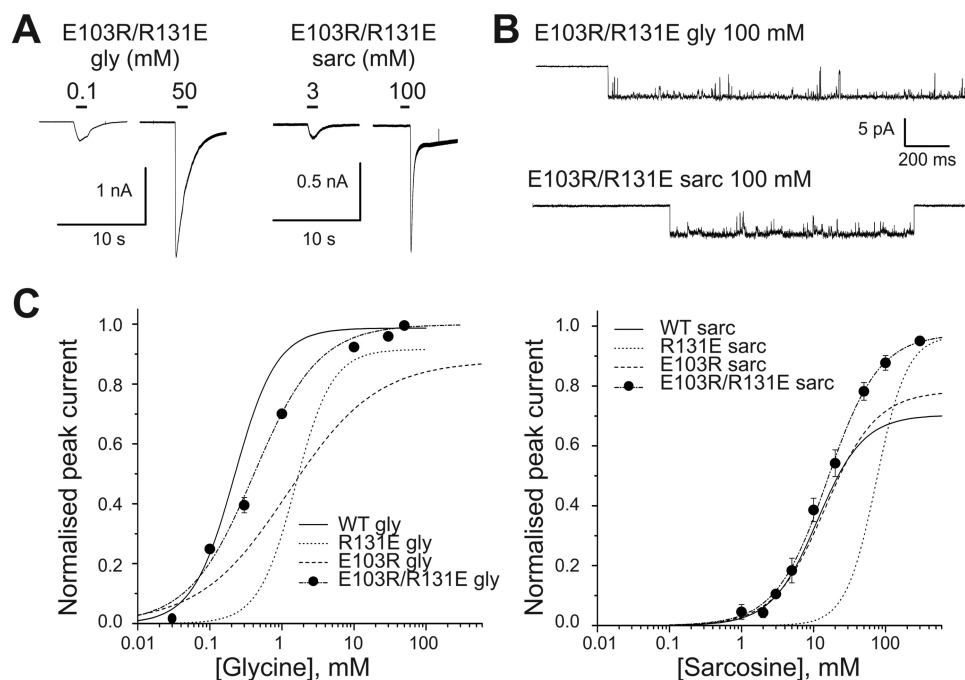


FIGURE 5. E103R/R131E mutation rescues $\alpha 1$ GlyR response to glycine and sarcosine. *A*, representative whole cell current responses to glycine or sarcosine in the double charge reversal mutant E103R/R131E GlyR $\alpha 1$. *B*, clusters of single-channel mutant GlyR activity elicited in cell-attached patches by saturating concentrations of glycine and sarcosine, respectively. *C*, glycine and sarcosine whole cell concentration-response curves in WT and double mutant GlyR ($n = 5$ and 8 , respectively). Curves are scaled to the appropriate maximum P_{open} measured by single channel recording. The WT concentration-response curves and the single-mutation curves for both glycine and sarcosine are shown for comparison (solid line for WT; the data for this curve is shown in Fig. 2C).

cacy is reflected by the increase in microscopic affinity for the agonist as the channel enters the pre-open intermediate state. Our data suggest that E103K must reduce this affinity increase, while leaving the basal affinity (for the resting state) unchanged. A great deal more molecular dynamics simulation data with the two agonists will be required to clarify how this effect maps to structure and the binding domain changes with activation. Further probing the role of this residue with conventional mutagenesis is limited by the restricted range of replacement side chains that can be introduced. Nevertheless, we found that mutating this residue to Arg instead of Lys had a much greater effect on glycine potency, with at least a 16-fold decrease. This effect is no longer purely on gating, but must impair also resting binding affinity, perhaps because the greater bulk of the positively charged side chain of Arg *versus* Lys causes some repacking. Employing unnatural amino acid mutagenesis to produce subtler side chain changes is likely to be needed.

Thus, despite its position in the binding site, startle disease mutation E103K acts by affecting channel gating, in line with other GlyR channelopathy mutations whose mechanism has been analyzed, such as K276E, A52S, and Q266H (10–12, 27), with the exception of N46K (14). We can estimate roughly the effects of E103K on a glycinergic synaptic current by calculating the time course and open probability of the channel in response to a synaptic glycine pulse (13). We used the rate constants in the mechanism we established for homomeric $\alpha 1$ GlyR (28) and reduced the forward rate constants of the initial conformational changes so that the mechanism reproduces the properties of E103K we observed here. We found that the main effect of the mutation is a substantial reduction in current amplitude, with a drop in peak P_{open} from 0.73 to 0.13. Our calculations were done for a homomeric GlyR, and synaptic GlyR are heteromers, but it is reasonable to assume that in heteromers we would see a similar functional impairment, perhaps mitigated by the presence of the WT β subunit.

Mutating Residues Glu-103 and Arg-131 Has Different Effects on Glycine and Sarcosine—Our single channel recordings gave direct measurements of agonist efficacy, but we found that the pattern of effects on the two agonists of the five single mutations and the double mutation was quite complex and hard to interpret in its entirety.

For glycine, charge reversal mutations produced loss-of-function phenotypes, which were somewhat different for Glu-103 and Arg-131. E103K produced a major decrease in glycine maximum P_{open} which, as discussed above, was not accompanied by detectable changes in affinity. Glycine is a very efficacious agonist on GlyR, with an E_{eff} of 70, and this makes it easier to detect losses of efficacy than gains in efficacy. Are we likely to miss increases in glycine opening efficacy (*cf.* the ones observed for sarcosine)? Given maximum $P_{\text{open}} = E_{\text{eff}}/(E_{\text{eff}} + 1)$, we would expect to be able to detect *decreases* in glycine efficacy greater than ~ 4 -fold. An increase in glycine efficacy cannot change the maximum P_{open} , but should still be detectable, because it is expected to increase the potency of glycine, as EC_{50} is inversely proportional to E_{eff} . The detection of such an effect could nevertheless be confounded by concurrent changes in K_d .

The situation is different for sarcosine. Sarcosine is a partial agonist (E_{eff} about 2.5), and therefore its maximum P_{open} should change clearly in response to both gain and loss of function mutations. For sarcosine, the effects of mutating Glu-103 were negligible for Ala or Arg mutations (Fig. 4C) and substantial for the Lys mutation (Fig. 2c), which we could not characterize completely because achieving saturating concentrations became osmotically impossible. Somewhat surprisingly, both of the two mutations tested for Arg-131 enhanced sarcosine gating, but the two mutations had opposite effects on potency: R131A increased sarcosine potency, but R131E decreased it, implying that R131E must cause also a decrease in sarcosine binding affinity. In contrast with that, R131E had produced a small loss in both efficacy and affinity for glycine. The differences in the effects of Arg-131 mutations on glycine and sarcosine efficacy show that the determinants of efficacy are different for the two agonists.

This is the first time that such different effects of a mutation on two agonists has been documented at single channel level for GlyR and shown to involve opposite changes in the efficacy of the two agonists. Other positions in loop A of GlyRs (Lys-104, Phe-108, and Thr-112) have been mutated in oocyte-expressed human $\alpha 1$ GlyR (29) in an alanine-scan and found to produce gain of function, general or confined to a subset of the agonists. These mutations are also likely to affect gating, as they increased the maximum whole cell response to the partial agonist taurine (relative to glycine).

Is Glu-103 Forming a Salt Bridge with Arg-131?—Both our homology model and the recent structural information on GlyR are consistent with the possibility that the side chains of loop A residue Glu-103 and loop E residue Arg-131 may form a salt bridge at the back of the agonist binding site and our data on the whole support the existence of this salt bridge.

The strongest evidence in favor comes from the double mutant experiments, in which swapping the side chains of residues Glu-103 and Arg-131 rescued most of the effects of the single point mutations. The exception was the increase in sarcosine efficacy seen with Arg-131 single mutations, which persisted in the double mutant. We do not know why this is the case. In the double mutant, the salt bridge may have the right length, but the interacting charged moieties (guanidinium in Arg and carboxylate in glutamate) should be in a different position, and lie closer to the complementary side of the site. Against the salt bridge hypothesis is the finding that eliminating the charge on either residue (by Ala mutations) had practically no effect on the GlyR activation by glycine. In any mutant, it is possible that the bond that we try to disrupt is replaced by a different interaction, but we are entering the realms of speculation.

Our data show that it is not easy to understand the network of interactions at the binding site even if we have unambiguous measurements of efficacy by single channel recording and a validated homology model. Exploring the salt bridge hypothesis further will require extensive molecular dynamics investigation of the conformation of the binding pocket, and how its interactions with different agonists change as the channel activates. This will require a large amount of simulation that we have just begun and which is beyond the scope of the current paper. These investigations would then suggest additional functional

experiments, which could include subtler residue changes with unnatural mutagenesis, and the formation of covalent disulfide bonds on activation.

Experimental Procedures

Homology Modeling—The human $\alpha 1$ GlyR model was constructed from the structure of *Danio rerio* $\alpha 1$ GlyR (glycine-bound open state; PDB code 3JAE) (17). The protein sequences for the two GlyRs (UniProt P23415 and O93430, respectively) were aligned using Muscle (30) and edited manually. 100 models were created with MODELLER version 9.16 (31) and out of the intersection of the top 10 of both DOPE score (32) and molecular PDF (31) the model with the best QMEAN score (33) was chosen for simulation. The termini of the model were capped with N-terminal acetyl and C-terminal acetamide with Maestro (Schrödinger Release 2013-2, Ref. 58) and hydrogens were added to the protein with the pdb2gmX tool of Gromacs 5.1 (34), assigning all side chains a protonation state at physiological pH (7.4).

Ligand Docking and Parameterization—The structures of the ligands glycine and sarcosine were taken from the ZINC ligand database (35). For each ligand and binding pocket, 50 binding modes were generated on a spherical search space of 12 Å diameter centered on the aromatic box with the docking program Gold (36) and the best-ranked one of each was selected as the final pose. The ligands were parameterized with AM1-BCC charges (37) and parameters from the general Amber force field (38) using ACPYPE (39).

System Set Up—Simulations were set up using a coarse-grained approach with the Martini force field version 2.2 using martinize (40) to coarse-grain the protein model. The overall systems were set up in a hexagonal prism as the periodic simulation box using insane (41), inserting the protein model in a 1-palmitoyl-2-oleoyl-*sn*-glycero-phosphocholine (POPC) bilayer, solvating in water, and adding sodium and chloride ions to neutralize the net charge and simulate a physiological concentration of 150 mM. Gromacs 5.1.x (34) was used for energy minimization and subsequent 500-ps constant temperature, constant volume (NVT)-, and 1- μ s constant temperature, constant pressure (NPT) equilibration. Simulation details were based on the recommended new-rf.mdp parameters (42) and appropriately adjusted. The final frame was then converted to all-atom resolution via backward (43). The original all-atom protein model was substituted into the system with the ligands in the poses predicted by docking.

All Atom Molecular Dynamics (MD) Simulations—The energy minimization and dynamics simulations were performed using Gromacs 5.1.x (34) and the following force fields: AMBER99SB-ILDN (44) for protein and ions, TIP3P for water (45), Slipids (46–48) for lipids, and the general Amber force field (38) for the ligands. Periodic boundary conditions in all three spatial dimensions were applied. Each system was energy-minimized using the steepest descent algorithm until the maximum force fell below 1000 kJ mol⁻¹ nm⁻¹. During all phases of equilibration, position restraints were applied to the protein heavy atoms and all ligand atoms with a force constant of 1000 kJ mol⁻¹ nm⁻². 100 ps of NVT equilibration at 310 K were followed by 30-ns NPT equilibration at 1 bar. Production runs

were run with no restraints for 500 ns in the NPT-ensemble. The van der Waals interactions were cut off at 1.0 nm and a dispersion correction was applied to energy and pressure. Electrostatic interactions were treated using the smooth Particle Mesh Ewald method (49, 50), where the real space contribution was cut off at 1.0 nm and the reciprocal energy term obtained in *k*-space was calculated on a grid with 0.12 nm spacing using 4th order B-splines for interpolation. The Verlet cut-off scheme was used to generate a pair-list with buffering using a tolerance of 0.005 kJ/mol/ps for pair-interactions per particle. All bonds involving hydrogens were constrained with the LINCS algorithm (51), allowing for a time step of 2 fs (only in the NVT equilibration a shorter time step of 1 fs was used). Temperature was maintained at constant physiological 310 K using the Bussi thermostat (52) with a coupling constant of 0.1 ps. In all isobaric simulations a barostat was coupled to the system in a semi-isotropic manner to maintain a pressure of 1 bar with a 1-ps coupling constant and the isothermal compressibility set to 4.5×10^{-5} bar⁻¹. The Berendsen barostat (53) was used in the NPT equilibration runs and the Parrinello-Rahmann barostat (54) for production runs.

Heterologous Expression in Human Embryonic Kidney Cells—Human embryonic kidney 293 cells (HEK 293) (from American Type Culture Collection) were grown at 37 °C in a humidified 95% air, 5% CO₂ incubator in Dulbecco's modified Eagle's medium (DMEM; Gibco) supplemented with 10% (v/v) heat-inactivated fetal bovine serum, 100 units/ml of penicillin G, 100 μ g/ml of streptomycin sulfate, and 2 mM L-glutamine (all from Invitrogen). Cells were passaged after reaching 70–80% confluence, every 2–3 days, up to 30 times.

Cells were plated on poly-L-lysine-coated glass coverslips (Sigma and VWR, respectively) in 35-mm culture dishes (Scientific Laboratory Supplies, SLS) containing 2 ml of DMEM, and were then transfected by the calcium phosphate-precipitation method (55) with pcDNA3.1 plasmids, one coding for the human glycine receptor subunit $\alpha 1$ (GenBank™ number P23415) and one coding for the enhanced green fluorescent protein (eGFP) to allow detection of transfected cells. In addition to that, empty pcDNA3.1 plasmid was added to ensure optimum expression levels. The proportion of empty plasmid varied depending on the channel expressed. For wild type channels, the final DNA mixture contained 2% GlyR $\alpha 1$ cDNA, 18% eGFP cDNA, and 80% empty pcDNA3.1 plasmid. The total amount of final DNA mixture was 3 μ g/plate. The transfection medium was washed off and replaced by fresh DMEM 4 h after transfection. Electrophysiological experiments were performed 1–2 days after transfection.

Point mutations were introduced using the QuikChange site-directed mutagenesis kit (Stratagene). Mutant sequences were confirmed by sequencing of the full open reading frame by Source BioScience LifeSciences (Nottingham, UK).

Whole Cell Recordings—These were obtained at least 24 h after transfection. Patch-pipettes were pulled from thick-walled borosilicate glass (GC150F; Harvard Apparatus, Edenbridge, UK) with a Sutter P-97 pipette puller (Sutter Instruments Co.) and fire-polished to a resistance of 3–5 M Ω when filled with internal solution containing (in mM): 101.1 potassium gluconate, 11 EGTA, 1 CaCl₂, 1 MgCl₂, 10 HEPES, 20

tetraethylammonium chloride (TEA-Cl), 2 MgATP, 40 glucose, and 6 KCl; the pH was adjusted to 7.4 with NaOH. All solutions were filtered through a 0.2- μ m Cyclopore track-etched membrane (GE Healthcare UK Ltd., Little Chalfont, UK) to remove impurities. The access resistance was below 10 M Ω and compensated by at least 70%. The bath solution contained (in mM): 20 Na gluconate, 112.7 NaCl, 2 KCl, 2 CaCl₂, 1.2 MgCl₂, 10 HEPES, 10 TEA-Cl, and 30 glucose; the pH was adjusted to 7.4 with NaOH. Whole cell currents were elicited by agonist application via U-tube application (56) and were recorded at a nominal holding potential of -50 mV with an AxoPatch 200B amplifier (Molecular Devices). The actual holding potential, corrected for the junction potential of 11 mV (calculated in pClamp10; Molecular Devices), was -61 mV. Recordings were prefiltered at 5 kHz with a four-pole low-pass Bessel filter, digitized at sampling rate of 20 kHz with a Digidata 1322A, and stored directly on a computer hard drive via Clampex10.2 software (all Molecular Devices).

The U-tube position was optimized before the experiment by the application of diluted bath solution (e.g. 50:50, bath solution:water) to an open tipped recording pipette, until the 10–90% exchange time was better than 100 ms. Average exchange time was less than 50 ms. A full concentration-response curve was obtained in each cell. To monitor the rundown/up of responses during recording, a standard concentration of agonist (usually saturating concentration) was applied every third or fourth response. Only cells in which rundown was less than 30% were accepted for further analysis and no correction for rundown was applied. The Hill equation was fitted to each individual concentration-response curve (program CVFIT; <https://github.com/DCPROGS>), to estimate EC₅₀ and n_H values. For the purpose of display only, responses were then normalized to the fitted maximum in each cell. These normalized responses were pooled and refitted with the Hill equation for the display.

Single-channel Recordings—These were obtained in the cell-attached configuration at least 24 h after transfection. Extracellular solution was made with HPLC-grade water, filtered through a 0.2- μ m Cyclopore track-etched membrane (GE Healthcare UK Ltd., Little Chalfont, UK) and contained (mM): 102.7 sodium gluconate, 4.7 KCl, 2 CaCl₂, 1.2 MgCl₂, 10 HEPES, 14 glucose, 15 sucrose, 20 TEA-Cl (from Sigma); the pH was adjusted to 7.4 with NaOH; osmolarity at 320 mOsm. Sylgard-coated thick-walled borosilicate pipettes fire-polished to a resistance of 10–15 M Ω were filled with extracellular solution containing a saturating concentration of agonist. Patches were voltage-clamped at a pipette potential of $+100$ mV with an Axopatch 200B amplifier. Data were pre-filtered at 10 kHz with the amplifier four-pole Bessel filter, digitized at 100 kHz with a Digidata 1322A and Clampex 10.2 (Molecular Devices) directly on the computer hard drive. Data were digitally filtered (low-pass Gaussian filter) to a final cut-off frequency of 4–6 kHz. At high agonist concentrations openings occurred in clusters delimited by long closed (desensitized) intervals (see Fig. 2B). Clusters are likely to originate from the activity of a single ion channel molecule and were used for P_{open} measurements (57), selecting clusters longer than 100 ms and with more than 10 openings. First, channel activity in the selected clusters was

idealized by half-amplitude threshold method (Clampfit 10.2, Molecular Devices). Open probability was calculated as the ratio of cluster open time over total cluster length. The single-channel current amplitude was calculated as a difference between the full open level (at the beginning of each cluster; 0.1 to 10 ms stretches) and the baseline (just before each cluster; 10 ms stretches).

The open probability response to a glycine concentration pulse that approximates synaptic conditions was calculated assuming an instantaneous rise to 3 mM glycine, followed by an exponential decay with a time constant of 2.5 ms (13). Rate constants used in the calculation are those obtained by global mechanism fit to rat $\alpha 1$ GlyR (28). The effect of the E103K mutation was approximated by reducing by 100-fold each of the three forward rate constants for flipping ($\delta 1$, $\delta 2$, and $\delta 3$). The resulting GlyR would have a maximum P_{open} of 0.75 and an EC₅₀ of 1.15 mM (cf. 0.73 and 0.71 mM measured for the E103K GlyR). Calculations were done using SCALCS. A Jupyter notebook with calculations is deposited in the SCALCS Git repository (https://github.com/DCPROGS/SCALCS/blob/master/notebooks/Calculate_Popen_SynapticCurrent_alpha1GlyR_Flip.ipynb). All electrophysiological recordings were carried out at a temperature of 19–21 °C.

Sarcosine was tested at 100 mM for glycine contamination by an HPLC assay: samples were resuspended in 10 μ l of 50% EtOH and reacted for 30 min with the following reagent: 90% EtOH:triethylamine:phenylisothiocyanate (7:2:1). They were then evaporated to dryness at room temperature and redissolved in 100 μ l of 5% acetonitrile in 0.1 M ammonium acetate. A 150 \times 4.6-mm Hypersil C18 column was used. Molecules of interest were detected at 254 nm. Sarcosine (Sigma) was found to be contaminated by about 10 μ M glycine per 100 mM. Sarcosine (approximately 7 g) was therefore purified by re-crystallizing it three times with 95% ethanol obtaining 2.37 g of purified compound, whose ¹H NMR and elemental analysis were consistent with those expected for sarcosine. The glycine contamination of a 100 mM solution of purified sarcosine was below the detection limit of the HPLC assay (about 1 μ M).

Author Contributions—F. S., E. H., M. E., T. G., and R. L. conducted patch clamp experiments; F. S. and R. L. analyzed experiments; R. L. made the patch clamp figures; M. W. I., G. F., and D. J. purified sarcosine; R. Y., M. A. D., and P. C. B. conducted molecular dynamics simulations and made Fig. 1; L. G. S., R. L., and P. C. B. designed experiments; L. G. S. wrote most of the paper with P. C. B. All authors reviewed the results and approved the final version of the manuscript.

Acknowledgment—We are grateful to Dr. Cali Hyde, Deltadot Bioanalysis Ltd., London NW1 0NH, for carrying out the HPLC analysis of the agonists.

References

1. Lynagh, T., and Pless, S. A. (2014) Principles of agonist recognition in Cys-loop receptors. *Front. Physiol.* 5, 160
2. Galzi, J.-L., and Changeux, J.-P. (1995) Neuronal nicotinic receptors: molecular organization and regulations. *Neuropharmacology* 34, 563–582
3. Zhong, W., Gallivan, J. P., Zhang, Y., Li, L., Lester, H. A., and Dougherty, D. A. (1998) From ab initio quantum mechanics to molecular neurobiol-

- ogy: a cation- π binding site in the nicotinic receptor. *Proc. Natl. Acad. Sci. U.S.A.* **95**, 12088–12093
4. Beene, D. L., Brandt, G. S., Zhong, W., Zacharias, N. M., Lester, H. A., and Dougherty, D. A. (2002) Cation- π interactions in ligand recognition by serotonergic (5-HT_{3A}) and nicotinic acetylcholine receptors: the anomalous binding properties of nicotine. *Biochemistry* **41**, 10262–10269
5. Pless, S. A., Millen, K. S., Hanek, A. P., Lynch, J. W., Lester, H. A., Lummis, S. C., and Dougherty, D. A. (2008) A cation- π interaction in the binding site of the glycine receptor is mediated by a phenylalanine residue. *J. Neurosci.* **28**, 10937–10942
6. Thompson, A. J., Lester, H., and Lummis, S. C. (2010) The structural basis of function in Cys-loop receptors. *Q. Rev. Biophys.* **43**, 1–51
7. Yu, R., Hurdiss, E., Greiner, T., Lape, R., Sivilotti, L., and Biggin, P. C. (2014) Agonist and antagonist binding in human glycine receptors. *Biochemistry* **53**, 6041–6051
8. Bode, A., and Lynch, J. W. (2014) The impact of human hyperekplexia mutations on glycine receptor structure and function. *Mol. Brain* **7**, 2
9. Lynch, J. W., Rajendra, S., Pierce, K. D., Handford, C. A., Barry, P. H., and Schofield, P. R. (1997) Identification of intracellular and extracellular domains mediating signal transduction in the inhibitory glycine receptor chloride channel. *EMBO J.* **16**, 110–120
10. Lewis, T. M., Sivilotti, L. G., Colquhoun, D., Gardiner, R. M., Schoepfer, R., and Rees, M. (1998) Properties of human glycine receptors containing the hyperekplexia mutation $\alpha 1$ (K276E), expressed in *Xenopus* oocytes. *J. Physiol.* **507**, 25–40
11. Moorhouse, A. J., Jacques, P., Barry, P. H., and Schofield, P. R. (1999) The startle disease mutation Q266H, in the second transmembrane domain of the human glycine receptor, impairs channel gating. *Mol. Pharmacol.* **55**, 386–395
12. Lape, R., Plested, A. J., Moroni, M., Colquhoun, D., and Sivilotti, L. G. (2012) The $\alpha 1$ K276E startle disease mutation reveals multiple intermediate states in the gating of glycine receptors. *J. Neurosci.* **32**, 1336–1352
13. Beato, M. (2008) The time course of transmitter at glycinergic synapses onto motoneurons. *J. Neurosci.* **28**, 7412–7425
14. Wilkins, M. E., Caley, A., Gielen, M. C., Harvey, R. J., and Smart, T. G. (2016) Murine startle mutant Nmf11 affects the structural stability of the glycine receptor and increases deactivation. *J. Physiol.* **594**, 3589–3607
15. Chung, S. K., Vanbellinghen, J. F., Mullins, J. G., Robinson, A., Hantke, J., Hammond, C. L., Gilbert, D. F., Freilinger, M., Ryan, M., Kruer, M. C., Masri, A., Gurses, C., Ferrie, C., Harvey, K., Shiang, R., *et al.* (2010) Pathophysiological mechanisms of dominant and recessive GLRA1 mutations in hyperekplexia. *J. Neurosci.* **30**, 9612–9620
16. Hibbs, R. E., and Gouaux, E. (2011) Principles of activation and permeation in an anion-selective Cys-loop receptor. *Nature* **474**, 54–60
17. Du, J., Lü, W., Wu, S., Cheng, Y., and Gouaux, E. (2015) Glycine receptor mechanism elucidated by electron cryo-microscopy. *Nature* **526**, 224–229
18. Moroni, M., Meyer, J. O., Lahmann, C., and Sivilotti, L. G. (2011) In glycine and GABA_A channels, different subunits contribute asymmetrically to channel conductance via residues in the extracellular domain. *J. Biol. Chem.* **286**, 13414–13422
19. Hansen, S. B., Wang, H. L., Taylor, P., and Sine, S. M. (2008) An ion selectivity filter in the extracellular domain of Cys-loop receptors reveals determinants for ion conductance. *J. Biol. Chem.* **283**, 36066–36070
20. Zhang, H. X., Lyons-Warren, A., and Thio, L. L. (2009) The glycine transport inhibitor sarcosine is an inhibitory glycine receptor agonist. *Neuropharmacology* **57**, 551–555
21. Beato, M., Groot-Kormelink, P. J., Colquhoun, D., and Sivilotti, L. G. (2004) The activation of $\alpha 1$ homomeric glycine receptors. *J. Neurosci.* **24**, 895–906
22. Lape, R., Colquhoun, D., and Sivilotti, L. G. (2008) On the nature of partial agonism in the nicotinic receptor superfamily. *Nature* **454**, 722–727
23. Colquhoun, D. (1998) Binding, gating, affinity and efficacy: the interpretation of structure-activity relationships for agonists and of the effects of mutating receptors. *Br. J. Pharmacol.* **125**, 924–947
24. Mukhtasimova, N., Lee, W. Y., Wang, H. L., and Sine, S. M. (2009) Detection and trapping of intermediate states priming nicotinic receptor channel opening. *Nature* **459**, 451–454
25. Jadey, S., and Auerbach, A. (2012) An integrated catch-and-hold mechanism activates nicotinic acetylcholine receptors. *J. Gen. Physiol.* **140**, 17–28
26. Sivilotti, L., and Colquhoun, D. (2016) In praise of single channel kinetics. *J. Gen. Physiol.* **148**, 79–88
27. Plested, A. J., Groot-Kormelink, P. J., Colquhoun, D., and Sivilotti, L. G. (2007) Single channel study of the spasmodic mutation $\alpha 1$ A52S in recombinant rat glycine receptors. *J. Physiol.* **581**, 51–73
28. Burzomato, V., Beato, M., Groot-Kormelink, P. J., Colquhoun, D., and Sivilotti, L. G. (2004) Single-channel behavior of heteromeric $\alpha 1\beta$ glycine receptors: an attempt to detect a conformational change before the channel opens. *J. Neurosci.* **24**, 10924–10940
29. Schmieden, V., Kuhse, J., and Betz, H. (1999) A novel domain of the inhibitory glycine receptor determining antagonist efficacies: further evidence for partial agonism resulting from self-inhibition. *Mol. Pharmacol.* **56**, 464–472
30. Edgar, R. C. (2004) MUSCLE: multiple sequence alignment with high accuracy and high throughput. *Nucleic Acids Res.* **32**, 1792–1797
31. Sali, A., and Blundell, T. L. (1993) Comparative protein modelling by satisfaction of spatial restraints. *J. Mol. Biol.* **234**, 779–815
32. Shen, M. Y., and Sali, A. (2006) Statistical potential for assessment and prediction of protein structures. *Protein Sci.* **15**, 2507–2524
33. Benkert, P., Künzli, M., and Schwede, T. (2009) QMEAN server for protein model quality estimation. *Nucleic Acids Res.* **37**, W510–W514
34. Abraham, M. J., Murtola, T., Schulz, R., Páll, S., Smith, J. C., Hess, B., and Lindahl, E. (2015) GROMACS: high performance molecular simulations through multi-level parallelism from laptops to supercomputers. *SoftwareX* **1–2**, 19–25
35. Sterling, T., and Irwin, J. J. (2015) ZINC 15: ligand discovery for everyone. *J. Chem. Inf. Model.* **55**, 2324–2337
36. Jones, G., Willett, P., Glen, R. C., Leach, A. R., and Taylor, R. (1997) Development and validation of a genetic algorithm for flexible docking. *J. Mol. Biol.* **267**, 727–748
37. Jakalian, A., Jack, D. B., and Bayly, C. I. (2002) Fast, efficient generation of high-quality atomic charges: AM1-BCC model: II. parameterization and validation. *J. Comput. Chem.* **23**, 1623–1641
38. Wang, J., Wolf, R. M., Caldwell, J. W., Kollman, P. A., and Case, D. A. (2004) Development and testing of a general amber force field. *J. Comput. Chem.* **25**, 1157–1174
39. Sousa da Silva, A. W., and Vranken, W. F. (2012) ACPYPE, AnteChamber Python Parser interface. *BMC Res. Notes* **5**, 367
40. de Jong, D. H., Singh, G., Bennett, W. F., Arnarez, C., Wassenaar, T. A., Schäfer, L. V., Periole, X., Tieleman, D. P., and Marrink, S. J. (2013) Improved parameters for the Martini coarse-grained protein force field. *J. Chem. Theory Comput.* **9**, 687–697
41. Wassenaar, T. A., Ingólfsson, H. I., Böckmann, R. A., Tieleman, D. P., and Marrink, S. J. (2015) Computational lipidomics with insane: a versatile tool for generating custom membranes for molecular simulations. *J. Chem. Theory Comput.* **11**, 2144–2155
42. de Jong, D. H., Baoukina, S., Ingólfsson, H. I., and Marrink, S. J. (2016) Martini straight: boosting performance using a shorter cutoff and GPUs. *Comp. Phys. Commun.* **199**, 1–7
43. Wassenaar, T. A., Pluhackova, K., Böckmann, R. A., Marrink, S. J., and Tieleman, D. P. (2014) Going backward: A flexible geometric approach to reverse transformation from coarse grained to atomistic models. *J. Chem. Theory Comput.* **10**, 676–690
44. Lindorff-Larsen, K., Piana, S., Palmo, K., Maragakis, P., Klepeis, J. L., Dror, R. O., and Shaw, D. E. (2010) Improved side-chain torsion potentials for the Amber ff99SB protein force field. *Proteins* **78**, 1950–1958
45. Jorgensen, W. L., Chandrasekar, J., Madura, J. D., Impey, R. W., and Klein, M. L. (1983) Comparison of simple potential functions for simulating liquid water. *J. Chem. Phys.* **79**, 926–935
46. Jämbek, J. P., and Lyubartsev, A. P. (2013) Another piece of the membrane puzzle: extending lipids further. *J. Chem. Theory Comput.* **9**, 774–784

47. Jämbäck, J. P., and Lyubartsev, A. P. (2012) An extension and further validation of an all-atomistic force field for biological membranes. *J. Chem. Theory Comput.* **8**, 2938–2948
48. Jämbäck, J. P., and Lyubartsev, A. P. (2012) Derivation and systematic validation of a refined all-atom force field for phosphatidylcholine lipids. *J. Phys. Chem. B* **116**, 3164–3179
49. Darden, T., York, D., and Pedersen, L. (1993) Particle mesh Ewald: an $N \cdot \log(N)$ method for Ewald sums in large systems. *J. Chem. Phys.* **98**, 10089–10092
50. Essmann, U., Perera, L., Berkowitz, M. L., Darden, T., Lee, H., and Pedersen, L. G. (1995) A smooth particle mesh Ewald method. *J. Chem. Phys.* **103**, 8577–8593
51. Hess, B., Bekker, H., Berendsen, H. J. C., Fraaije, J. G. E. M. (1997) LINCS: a linear constraint solver for molecular simulations. *J. Comp. Chem.* **18**, 1463–1472
52. Bussi, G., Donadio, D., and Parrinello, M. (2007) Canonical sampling through velocity rescaling. *J. Chem. Phys.* **126**, 014101
53. Berendsen, H. J. C. (2007) *Simulating the Physical World: Hierarchical modeling from quantum mechanics to fluid dynamics*, Cambridge University Press, Cambridge, United Kingdom
54. Parrinello, M., and Rahman, A. (1981) Polymorphic transitions in single crystals: a new molecular dynamics method. *J. Appl. Phys.* **52**, 7182–7190
55. Groot-Kormelink, P. J., Beato, M., Finotti, C., Harvey, R. J., and Sivilotti, L. G. (2002) Achieving optimal expression for single channel recording: a plasmid ratio approach to the expression of $\alpha 1$ glycine receptors in HEK293 cells. *J. Neurosci. Methods* **113**, 207–214
56. Krishtal, O. A., and Pidoplichko, V. I. (1980) A receptor for protons in the nerve cell membrane. *Neuroscience* **5**, 2325–2327
57. Sivilotti, L. G. (2010) What single channel analysis tells us of the activation mechanism of ligand-gated channels: the case of the glycine receptor. *J. Physiol.* **588**, 45–58
58. Schrödinger, LLC. (2013) *Maestro, version 9.5*, Schrödinger, LLC., New York

The Startle Disease Mutation E103K Impairs Activation of Human Homomeric $\alpha 1$ Glycine Receptors by Disrupting an Intersubunit Salt Bridge across the Agonist Binding Site

Fatemah Safar, Elliot Hurdiss, Marios Erotocritou, Timo Greiner, Remigijus Lape, Mark W. Irvine, Guangyu Fang, David Jane, Rilei Yu, Marc A. Dämgen, Philip C. Biggin and Lucia G. Sivilotti

J. Biol. Chem. 2017, 292:5031-5042.

doi: 10.1074/jbc.M116.767616 originally published online February 7, 2017

Access the most updated version of this article at doi: [10.1074/jbc.M116.767616](https://doi.org/10.1074/jbc.M116.767616)

Alerts:

- [When this article is cited](#)
- [When a correction for this article is posted](#)

[Click here](#) to choose from all of JBC's e-mail alerts

This article cites 55 references, 16 of which can be accessed free at <http://www.jbc.org/content/292/12/5031.full.html#ref-list-1>